

Fluorophosphates from Solid-State Synthesis and Electrochemical Ion Exchange: NaVPO_4F or $\text{Na}_3\text{V}_2(\text{PO}_4)_2\text{F}_3$?

Long Li, Youlong Xu,* Xiaofei Sun, Rui Chang, Yuan Zhang, Xiaona Zhang, and Ju Li*

Vanadium-based fluorophosphates are promising sodium-ion battery cathode materials. Different phases of NaVPO_4F and $\text{Na}_3\text{V}_2(\text{PO}_4)_2\text{F}_3$ are reported in the literature. However, experiments in this work suggest that there could be confusions about the single-phase NaVPO_4F in solid-state synthesis. Here, systematic investigation of the mechanism underlying structural and compositional evolution of solid-state synthesis ($\text{NaF}:\text{VPO}_4 = 1:1$) is determined by in situ and ex situ X-ray diffraction and electrochemical measurements. Three reactions— $3\text{NaF} + 3\text{VPO}_4 \rightarrow \text{Na}_3\text{V}_2(\text{PO}_4)_2\text{F}_3 + \text{VPO}_4$ (up to 500 °C), $\text{Na}_3\text{V}_2(\text{PO}_4)_2\text{F}_3 + \text{VPO}_4 \rightarrow \text{Na}_3\text{V}_2(\text{PO}_4)_3 + \text{VF}_3\uparrow$ (600–800 °C), and $2\text{Na}_3\text{V}_2(\text{PO}_4)_3 \rightarrow 2(\text{VO})_2\text{P}_2\text{O}_7 + \text{Na}_4\text{P}_2\text{O}_7 + \text{amorphous products}$ (above 800 °C)—are validated by in situ XRD and thermogravimetric analysis/differential scanning calorimetry. None of the products reported in this work is consistent with single-phase NaVPO_4F at any temperature. It is speculated that the assignments of I_4/mmm and C_2/c NaVPO_4F from solid-state synthesis are incorrect, which are instead multiphase mixtures of Le Meins' $\text{Na}_3\text{V}_2(\text{PO}_4)_2\text{F}_3$, unreacted VPO_4 , and hexagonal $\text{Na}_3\text{V}_2(\text{PO}_4)_3$. Liquid-electrolyte-based electrochemical ion exchange of LiVPO_4F produces a favorite NaVPO_4F structure, which is very different from Le Meins' family of $\text{Na}_3\text{Al}_2(\text{PO}_4)_2\text{F}_3$ polymorphs.

potential cathode materials for rechargeable SIBs.^[1c,2] Among these structures, NaVPO_4F ($\text{NaF}:\text{VPO}_4 = 1:1$) and $\text{Na}_3\text{V}_2(\text{PO}_4)_2\text{F}_3$ ($\text{NaF}:\text{VPO}_4 = 3:2$) were first shown by the Barker group in 2003 and 2006, respectively, as reversible insertion hosts for SIBs.^[3] Both were obtained by solid-state synthesis with stoichiometric proportions of reactants, namely, $\text{NaF}:\text{VPO}_4 = 1:1$ feedstock for NaVPO_4F , and $\text{NaF}:\text{VPO}_4 = 3:2$ feedstock for $\text{Na}_3\text{V}_2(\text{PO}_4)_2\text{F}_3$. Barker's original 2003 reference described the thus-obtained NaVPO_4F compound as tetragonal I_4/mmm ; but, it was mentioned in the same reference that the XRD pattern was “also in good accordance with the structural analysis of the related compound, $\text{Na}_3\text{Al}_2(\text{PO}_4)_2\text{F}_2$ ” [*sic*, the authors meant $\alpha\text{-Na}_3\text{Al}_2(\text{PO}_4)_2\text{F}_3$] despite the obvious difference in stoichiometry, also I_4/mmm , first described by Le Meins and co-workers in 1999, with $a = 6.206 \text{ \AA}$ and $c = 10.418 \text{ \AA}$.^[3a,4] This allegedly I_4/mmm

1. Introduction


Sodium-ion batteries (SIBs) are promising alternatives to lithium-ion batteries (LIBs) for large-scale energy storage.^[1] Due to the high operating voltage and thermal stability, vanadium-based fluorophosphates have aroused great interest as

NaVPO_4F was reported with a high average discharge potential of 3.7 V (vs hard carbon) and a specific capacity of 82 mAh g^{-1} (theoretical capacity should be 143 mAh g^{-1} if $\text{V}^{3+}/\text{V}^{4+}$ is fully utilized), which might be comparable to the commercial cathode material LiFePO_4 (3.4 V vs Li/Li^+ and theoretical capacity 170 mAh g^{-1}) of LIBs.^[3a,5] Since then, many groups have attempted to synthesize NaVPO_4F to improve its electrochemical performance.

L. Li, Prof. Y. Xu, Dr. X. Sun, Y. Zhang, X. Zhang
Electronic Materials Research Laboratory
Key Laboratory of the Ministry of Education & International
Center for Dielectric Research
Xi'an Jiaotong University
Xi'an 710049, P. R. China
E-mail: ylxu@mail.xjtu.edu.cn

L. Li, Prof. Y. Xu, Dr. X. Sun, R. Chang, Y. Zhang, X. Zhang
Shaanxi Engineering Research Center of Advanced Energy
Materials & Devices
Xi'an Jiaotong University
Xi'an 710049, P. R. China

Prof. J. Li
Department of Nuclear Science and Engineering and Department
of Materials Science and Engineering
Massachusetts Institute of Technology Cambridge
MA 02139, USA
E-mail: liju@mit.edu

 The ORCID identification number(s) for the author(s) of this article can be found under <https://doi.org/10.1002/aenm.201801064>.

DOI: 10.1002/aenm.201801064

template method which delivered high cycling stability.^[10] Details of the crystal structures and phase transition between tetragonal and monoclinic NaVPO₄F are confusing. Many of the works after Barker and co-workers and Zhuo and co-workers were based on the belief that monoclinic *C*₂/*c* and tetragonal *I*₄/*mmm* forms of NaVPO₄F exist as single-phase compound after 1:1 stoichiometric solid-state synthesis.^[3a,6,11]

Recently, Boivin and co-workers proposed a tavorite-type NaVPO₄F by liquid-phase hydrothermal synthesis.^[12] This structure is also monoclinic with space group of *C*₂/*c*. However, different from the previously stated structures with acclaimed (but puzzling) similarity to Le Meins family of Na₃Al₂(PO₄)₂F₃,^[3a,4,6,11] Boivin's structure is built up by VO₄F₂ octahedra chains connected to each other via PO₄ tetrahedra, similar to other tavorite-type compounds, such as LiVPO₄F, LiVPO₄OH, and HVPO₄OH. For clarity, in this paper we will denote the monoclinic structure pinned down by Boivin and co-workers as “tavorite type,” and the other monoclinic structure(s) as “nontavorite monoclinic” NaVPO₄F. Note that while the crystal drawing of tavorite NaVPO₄F was given by Boivin and co-workers,^[12] the crystal drawing of nontavorite *C*₂/*c* NaVPO₄F was not provided,^[6,11] nor was that of tetragonal *I*₄/*mmm* NaVPO₄F.^[3a] Thus, the nontavorite *C*₂/*c* and the tetragonal *I*₄/*mmm* forms of NaVPO₄F are mysterious to us.^[3a,6,11]

Barker and co-workers demonstrated in 2006 that Na₃V₂(PO₄)₂F₃ can provide 115–120 mAh g⁻¹ reversible capacity,^[3b] and was initially solved to be tetragonal *P*₄/*mmn*,^[3b] belonging to Le Meins' family of Na₃Al₂(PO₄)₂F₃ polymorphs that include the tetragonal *I*₄/*mmm* α-Na₃Al₂(PO₄)₂F₃, and can undergo temperature-driven massive transformations within this family.^[4] But its symmetry has been later revised and established as subtle orthorhombic (*b/a* = 1.002) space group *Amam* by Bianchini and co-workers by using a high angular resolution synchrotron diffraction, “preserving the global geometry of the *P*₄/*mmn* framework but showing a different distribution of sodium ions.”^[13] This crystal structure consists of pairs of corner-sharing VO₄F₂ octahedra, which are equatorially connected to PO₄ tetrahedra via O atoms. The doubt about the structural parallels between NaVPO₄F and Na₃Al₂(PO₄)₂F₃ despite obvious stoichiometry difference was suggested by Sauvage and co-workers^[14] Moreover, the clear difference in acclaimed lattice motifs in the two monoclinic NaVPO₄F with same materials stoichiometry and space group (Zhuo et al's and Boivin et al's) also fed our suspicion. Therefore, we initially seek to understand the formation mechanism and define the structure of NaVPO₄F.

Both powder and tablet samples were prepared via conventional solid-state synthesis method at temperatures from 550 to 750 °C. In situ X-ray diffraction (XRD) and thermogravimetric analysis/differential scanning calorimetry (TGA/DSC) measurements were employed to investigate the structural evolution details upon the heating process. The structural and compositional changes can be detected and quantified by recording spectra at a certain interval temperature. FT-IR, X-ray photoelectron spectroscopy (XPS), and high-resolution transmission electron microscopy (HRTEM) measurements were carried out to complement the XRD data. The structural and compositional evolution accompanied by detailed heating mechanisms during the electrochemical process was further evaluated.

2. Results and Discussion

The XRD pattern with Rietveld refinement of the precursor phase (*R*_p = 2.3%, *R*_{wp} = 3.2%) is presented in Figure S1a in the Supporting Information. VPO₄ (ICDD PDF No. 01-086-1196) without any impurities is indeed formed according to Equation (M1) in methods. The ex situ XRD patterns of the tablet samples (NaF:VPO₄ = 1:1) treated at various temperatures (TS550, TS600, TS650, TS700, and TS750) are shown in Figure 1a. XRD patterns are measured by mixing 5% silicon (ICDD PDF No. 01-089-2749) powder in these products to determine the exact composition of tablet samples. The results indicate that these samples are mainly composed of tetragonal Na₃V₂(PO₄)₂F₃ (ICDD PDF No. 01-089-8485) and VPO₄ below 650 °C. A new set of diffraction peaks of tablet samples can be indexed as the hexagonal crystalline Na₃V₂(PO₄)₃ (ICDD PDF No. 00-053-0018) above 600 °C, with a small amount of (VO)₂P₂O₇ (ICDD PDF No. 01-085-2281) and Na₄P₂O₇ (ICDD PDF No. 00-001-0356) byproducts. Upon further heating, a marked drop in the intensity of VPO₄ peaks and a gradual decline in Na₃V₂(PO₄)₂F₃ are also observed. Figure 1b depicts the Rietveld refinement of TS600 on the basis of the XRD data, revealing that TS600 consists of Na₃V₂(PO₄)₂F₃ and VPO₄ with space group of *P*₄/*mmn* and *Cmcm* (*R*_p = 3.9%, *R*_{wp} = 5.5%), respectively. We are not able to confirm or deny the subtle orthorhombic space group *Amam* assignment to Na₃V₂(PO₄)₂F₃ by Bianchini and co-workers (*b/a* = 1.002) due to the resolution of our instrument.^[13] Therefore, here we speculate that NaVPO₄F cannot be synthesized by solid-state synthesis at any temperature, and Na₃V₂(PO₄)₃ is part of the reaction products between Na₃V₂(PO₄)₂F₃ and VPO₄. The schematic crystal structures of the tetragonal *P*₄/*mmn*/ subtle orthorhombic (*b/a* = 1.002) *Amam* Na₃V₂(PO₄)₂F₃ and hexagonal *R* $\bar{3}$ *c* Na₃V₂(PO₄)₃ are shown in Figure 1c. Different from Na₃V₂(PO₄)₂F₃ with 3D structure of V₂O₈F₃ biotetrahedra bridged by PO₄ tetrahedra, Na₃V₂(PO₄)₃ is built by isolated VO₆ octahedra and PO₄ tetrahedra interlinked via corners to establish the framework anion [V₂(PO₄)₃]³⁻.^[15] To further confirm our speculation, a powdery raw materials mixture (NaF:VPO₄ = 1:1) is also calcined at similar temperatures. XRD patterns of these powder samples (PS550, PS600, PS650, PS700, PS750, and PS800) are shown in Figure S1b in the Supporting Information. The graph shows that there has been a sharper decreasing trend in the intensities of Na₃V₂(PO₄)₂F₃ peaks until they disappeared altogether in PS800, suggesting that the tablet sample impeded volatilization of fluorine and reaction between Na₃V₂(PO₄)₂F₃ and VPO₄. To further confirm the synthetic products, samples with increasing ratio of feed-stock NaF to VPO₄ (1.0:1 to 1.5:1) are calcined at 600 °C. As shown in Figure S1 in the Supporting Information, there is a steady downward trend in the intensity of XRD peaks related to VPO₄ until it disappears eventually upon increasing NaF to VPO₄ ratio, demonstrating that only Na₃V₂(PO₄)₂F₃ could be synthesized in solid-state synthesis.

To further understand crystal structure changes of the raw materials (NaF:VPO₄ = 1:1) from 25 to 950 °C, in situ XRD and TGA/DSC measurements are conducted (Figure 2). The heating process can be divided into four regimes by magenta lines in Figure 2: R1 for the preparation stage before solid-state reactions of raw materials below 400 °C, R2 for synthetic reaction

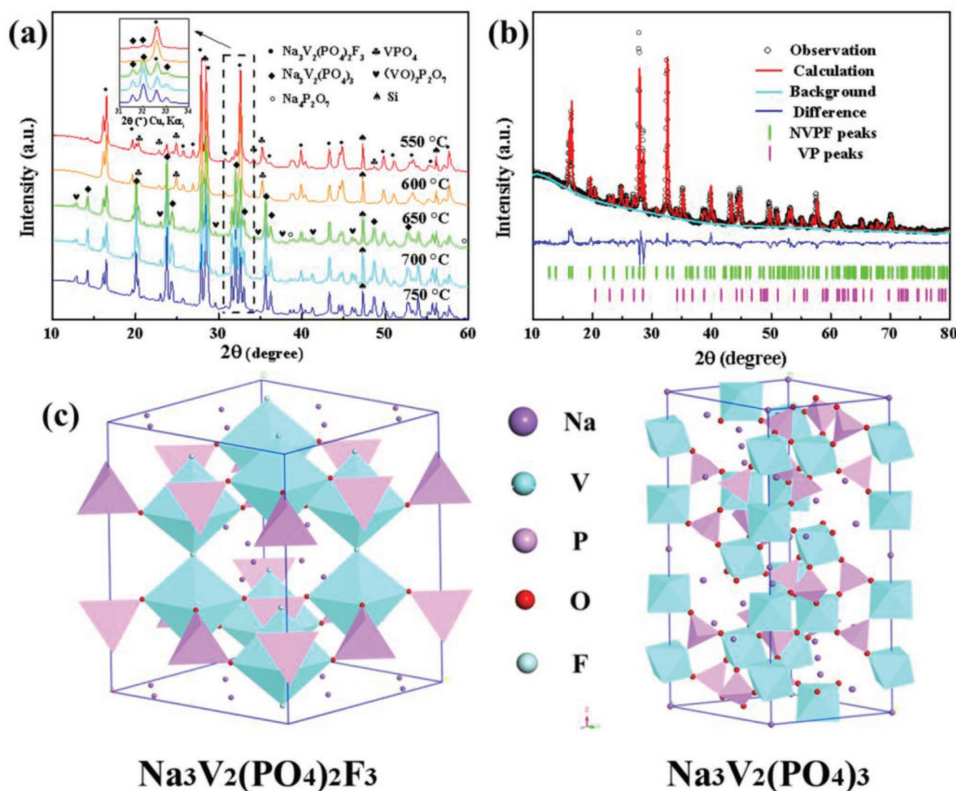


Figure 1. Crystal structure of $\text{Na}_3\text{V}_2(\text{PO}_4)_2\text{F}_3$ and $\text{Na}_3\text{V}_2(\text{PO}_4)_3$. a) XRD patterns of the tablet samples calcined at 550–750 °C. b) Rietveld refinement based on the XRD pattern of tablet sample calcined at 600 °C. Black circle, red line, cyan line, and blue line represent the observed, calculated, background, and difference patterns, respectively. The green and magenta tick marks correspond to the $\text{Na}_3\text{V}_2(\text{PO}_4)_2\text{F}_3$ and VPO_4 Bragg reflections, respectively. The abbreviation of NVPF and VP correspond to the $\text{Na}_3\text{V}_2(\text{PO}_4)_2\text{F}_3$ and VPO_4 . c) Schematic crystal structures of the tetragonal $P4_2/mnm$ /subtly orthorhombic ($b/a = 1.002$) $Amam$ $\text{Na}_3\text{V}_2(\text{PO}_4)_2\text{F}_3$ and hexagonal $R\bar{3}c$ $\text{Na}_3\text{V}_2(\text{PO}_4)_3$.

of feedstock materials from 400 to 700 °C, R3 for chemical reaction between $\text{Na}_3\text{V}_2(\text{PO}_4)_2\text{F}_3$ and VPO_4 from 700 to 850 °C, and R4 for decomposition reaction of $\text{Na}_3\text{V}_2(\text{PO}_4)_3$ above 850 °C. For clarity, only the characteristic diffraction peak areas of the phases: (002) peak of NaF (ICDD PDF No. 01-070-2508); (111) and (112) peaks of VPO_4 ; (002) peak of $\text{Na}_3\text{V}_2(\text{PO}_4)_2\text{F}_3$; (113), (116), and (226) peaks of $\text{Na}_3\text{V}_2(\text{PO}_4)_3$; (113) peak of $(\text{VO})_2\text{P}_2\text{O}_7$; and (005) peak of $\text{Na}_4\text{P}_2\text{O}_7$ are shown. Figure 2a displays the stacked in situ XRD patterns corresponding to TGA/DSC curves. Figure 2b shows the color-coded and temperature-resolved intensity plots. The reference color bar is located under each XRD peak/peak pair, respectively. In addition, specific proportions of different components during the compositional evolution by semiquantitative calculation are displayed versus temperature in Figure 3 and Table S1 in the Supporting Information.

In R1 regime, with the temperature increasing up to 300 °C, all diffraction peaks of NaF and VPO_4 shift toward low angles. This phenomenon results from lattice expansion triggered by the atomic diffusion. When temperature increases up to 400 °C, intensity of NaF (002) peak weakens prominently while intensity of VPO_4 (111) and (112) peaks declines as well but much slower, indicating the reaction between NaF and VPO_4 occurs and the consumption rate of NaF is greater than VPO_4 . The appearance of the new peak at 16.55° and the residual

peaks of unreacted VPO_4 affirms the tetragonal/orthorhombic $\text{Na}_3\text{V}_2(\text{PO}_4)_2\text{F}_3$ as a result of 3:2 reaction in a feedstock of 1:1 NaF and VPO_4 .

In R2 regime, the peak intensity of NaF keeps weakening until it disappears at 500 °C, while (002) peak of $\text{Na}_3\text{V}_2(\text{PO}_4)_2\text{F}_3$ continues to increase, indicating the synthetic reaction keeps proceeding until NaF runs out. It should be noted that the ratio of $\text{Na}_3\text{V}_2(\text{PO}_4)_2\text{F}_3$ and VPO_4 remains 1:1 until both of them exhausted at 800 °C, which matches the expected proportion after 3:2 synthetic reaction of $\text{Na}_3\text{V}_2(\text{PO}_4)_2\text{F}_3$, confirming the reaction product is $\text{Na}_3\text{V}_2(\text{PO}_4)_2\text{F}_3$ instead of tetragonal NaVPO_4F .

In R3 regime, from both stacked linear diffraction pattern and color-coded intensity plots in Figure 2, it is clear that the peak intensities of both $\text{Na}_3\text{V}_2(\text{PO}_4)_2\text{F}_3$ and VPO_4 significantly decline when temperature rises to 700 °C, whereas another series of new and strong peaks emerge, whose peak positions are nearly the same as the proposed monoclinic NaVPO_4F phase reported by many previous works.^[6,7,9b,11,16] To further investigate the new crystal structure, the TGA/DSC measurement corresponding to in situ XRD was employed. As shown in Figures 2 and 3, there are a remarkable weight loss ($\approx 6.6\%$) and a strong endothermic peak from 650 to 800 °C corresponding to the generation of the new peaks. This weight loss precludes the possibility of $\text{Na}_3\text{V}_2(\text{PO}_4)_2\text{F}_3 + \text{VPO}_4 = 3\text{NaVPO}_4\text{F}$. After careful comparison, these new peaks can be attributed to hexagonal

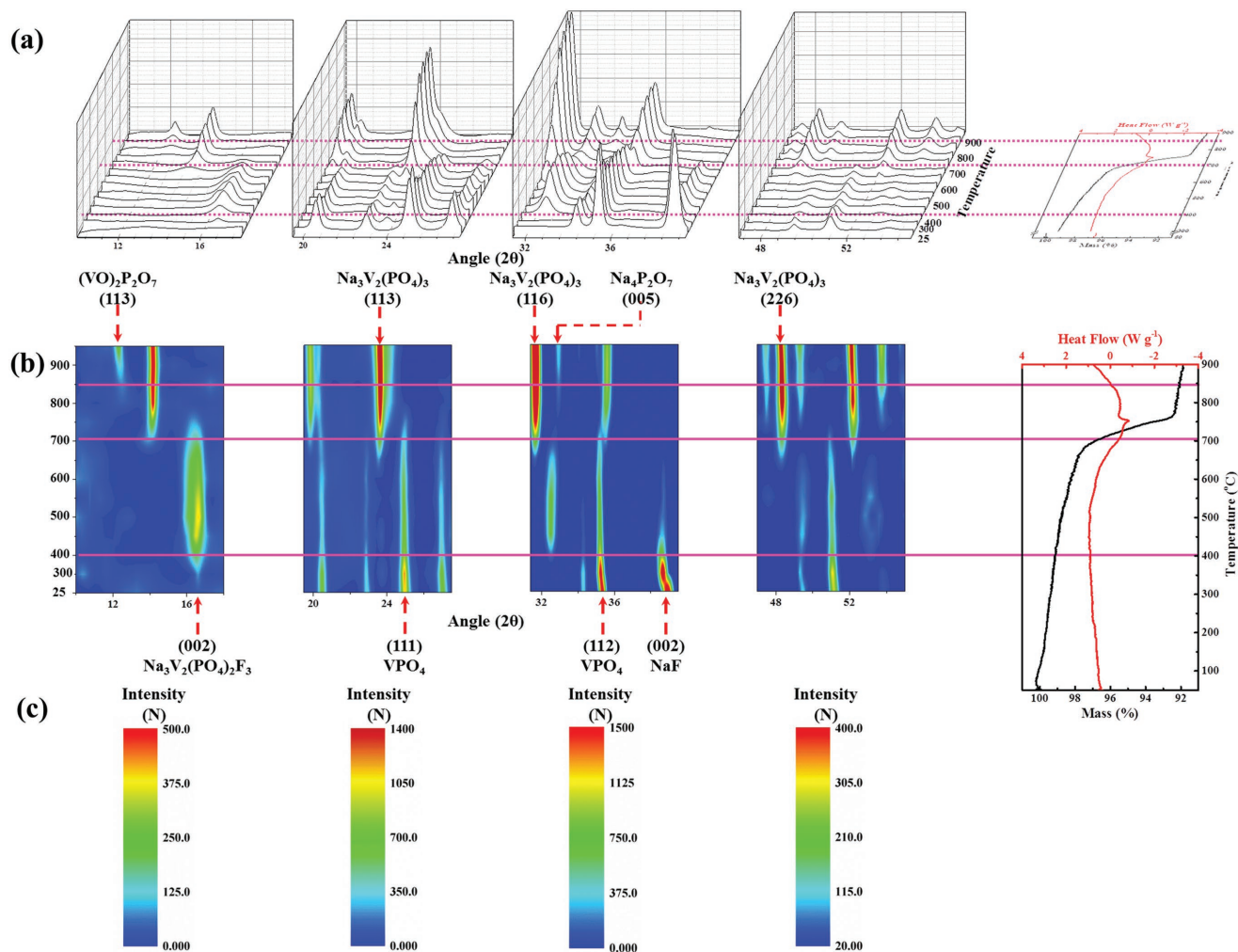


Figure 2. Structure and compositional evolution of raw materials upon heating. a) Selected area and stacked in situ XRD patterns correspond to the TGA/DSC curves. b) The color-coded, temperature-resolved, intensity distribution plots correspond to the TGA/DSC curves. c) The reference color bar.

$\text{Na}_3\text{V}_2(\text{PO}_4)_3$ (space group $R\bar{3}c$), with weight loss attributed to volatile VF_3 (gas). The $\approx 6.6\%$ weight loss is less than the theoretical proportion of VF_3 ($\approx 17.5\%$) because part of the VF_3 is obstructed by the coating layer of amorphous carbon.^[17] Therefore, tetragonal I_4/mmm and nontavorite monoclinic C_2/c NaVPO_4F may not exist. They might instead be tetragonal $P4_2/mnm$ /subtle orthorhombic ($b/a = 1.002$) Amm $\text{Na}_3\text{V}_2(\text{PO}_4)_2\text{F}_3$ and $R\bar{3}c$ $\text{Na}_3\text{V}_2(\text{PO}_4)_3$, respectively, shown in Figure 1c, depending on the thermal treatment temperature. Because of the loss of VF_3 , there can be no formation of or phase transition to nontavorite monoclinic C_2/c phase NaVPO_4F at still higher temperatures. Besides, pure rhombohedral $\text{Na}_3\text{V}_2(\text{PO}_4)_3$ are detected after complete chemical reaction at 800°C .

In R4, a progressive increase of several new peak intensities is observed at 850°C , satisfying the mechanism of Equation (3) occurring at high temperature.^[18] These new peaks can be attributed to the $(\text{VO})_2\text{P}_2\text{O}_7$ (113) reflection and $\text{Na}_4\text{P}_2\text{O}_7$ (005) peak after rigorous analysis. Therefore, rhombohedral $\text{Na}_3\text{V}_2(\text{PO}_4)_3$ cannot sustain temperature above 800°C and will decompose to $(\text{VO})_2\text{P}_2\text{O}_7$, $\text{Na}_4\text{P}_2\text{O}_7$, and maybe other amorphous products (APs) that we have not clarified yet.^[19] Due

to tableting of raw materials and gaseous reaction product, chemical reaction between $\text{Na}_3\text{V}_2(\text{PO}_4)_2\text{F}_3$ and VPO_4 is far from completed in TS750. To summarize, the structural and compositional evolution in synthesis process of raw materials can be described as follows

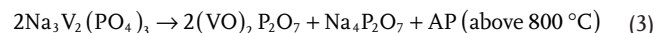
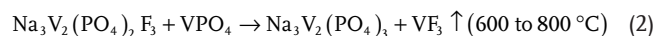
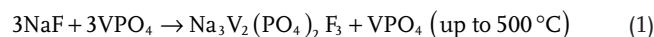


Figure 4 shows Fourier transform-infrared spectrum (FT-IR) spectra between 2400 and 400 cm^{-1} for as-synthesized products. The weak bands at 1650 and 1398 cm^{-1} can be ascribed to O–H bending and O–H vibration of C–OH groups.^[20] When the temperature rises, these two bands become weaker in powder samples (Figure S2, Supporting Information), but no such change occurs in the tablet samples. This phenomenon indicates tablet hinders the release of gases and the breakdown of C–OH groups. Strong broad band at 1060 cm^{-1} can be attributed to asymmetric

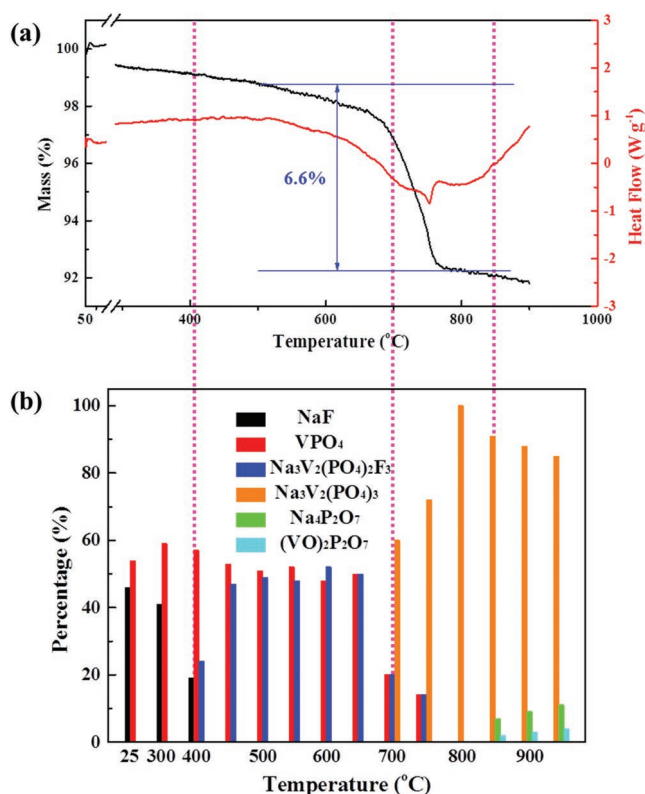


Figure 3. The specific compositional charges (atomic ratio) of raw materials upon heating. a) The TGA/DSC curves of raw materials upon heating from 50 to 900 °C in Ar flow. b) The corresponding specific compositional changes calculated by semiquantitative calculation of in situ XRD patterns.

stretching of PO_4^{3-} tetrahedron.^[21] The relative strength of the bands of absorbance of C–F bond at 1178 cm^{-1} , stretching vibration of V–F bond at 944 cm^{-1} , symmetric stretching mode of P–O bond at 673 cm^{-1} , vibration of $\text{P}_2\text{O}_7^{4-}$ unit at 602 cm^{-1} , and asymmetric bending vibration $\nu(\text{F}_2)$ of PO_4^{3-} at 556 cm^{-1} varies with the rising temperature.^[21,22] Stretching vibration of V–F bond (944 cm^{-1}) becomes weaker until it disappeared, whereas

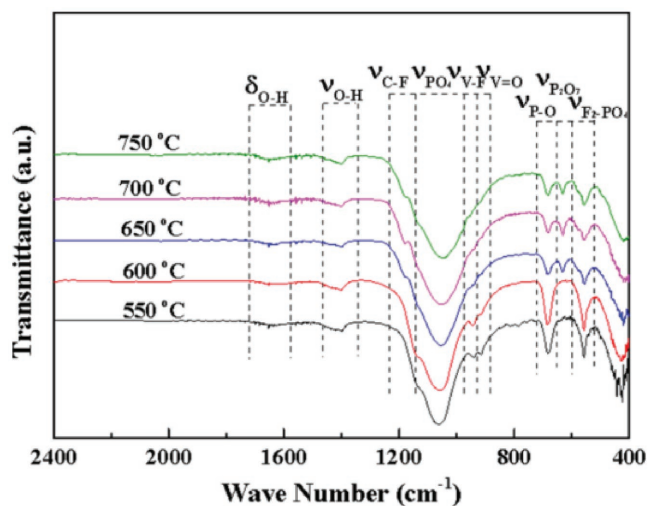


Figure 4. FT-IR spectra of tablet samples calcined at 550–750 °C.

absorbance of C–F bond (1178 cm^{-1}) becomes slightly stronger. It indicates that Equation (2) reaction is sustained and part of evaporable fluoride is captured by carbon coating layer. Furthermore, symmetric stretching of P–O bond (673 cm^{-1}) and asymmetric bending vibration $\nu(\text{F}_2)$ of PO_4^{3-} (556 cm^{-1}) keep lessening, whereas vibration of $\text{P}_2\text{O}_7^{4-}$ unit (602 cm^{-1}) intensifies along with the rising temperature above 650 °C . It means the $\text{V}_2\text{O}_8\text{F}_3$ bioctahedra in $\text{Na}_3\text{V}_2(\text{PO}_4)_2\text{F}_3$ transfers to isolated VO_6 octahedra in $\text{Na}_3\text{V}_2(\text{PO}_4)_3$ and the reaction product $\text{Na}_3\text{V}_2(\text{PO}_4)_3$ further decomposes as $\text{Na}_4\text{P}_2\text{O}_7$, $(\text{VO})_2\text{P}_2\text{O}_7$, and other AP. The much weaker intensity of bands at 944 and 556 cm^{-1} in powder samples obtained at 800 °C (Figure S2, Supporting Information) also demonstrates that compact tablet impedes the fluorine from fleeing the crystal lattice of $\text{Na}_3\text{V}_2(\text{PO}_4)_2\text{F}_3$. Overall, the peak shift and intensity in in situ and ex situ XRD patterns and the varying strength and position for bands in FT-IR spectra confirm that V–F bonds rupture in crystal, fluorine runs away from the $\text{Na}_3\text{V}_2(\text{PO}_4)_2\text{F}_3$, and part of PO_4^{3-} unit transfers into $\text{P}_2\text{O}_7^{4-}$ group, affirming that feedstock materials undergo three reactions (Equations (1)–(3)) upon heating.

X-ray photoelectron spectroscopy (XPS) analysis of tablet samples is shown in Figure 5. In the F 1s spectra, two components of F–C bond at 687.0 eV and F–V bond at 684.0 eV are observed. The intensity of F–V bond is gradually and significantly reduced, and F–C bond increased much slower as resultant temperature increases, illustrating that the group related to F–V bond is tapered off and only part of fluorine has been captured by the coating carbon layer.^[23] The C 1s region for tablet samples can be deconvoluted into five Gaussian peaks: C–C at 284.6 eV , C–O at 285.8 eV , C=O at 286.8 eV , O–C=O at 288.5 eV , and C–F at 289.0 eV .^[20b,23a,24] The same trend as F–C bond in F 1s region confirms the speculation about the evolution of groups related to fluorine analyzed by in situ XRD and FT-IR measurement. The P 2p spectra are characterized by a broadened band which can be decomposed in two different components at 133.9 eV for P=O bond and 132.9 eV for P–O bond. The intensity of the broadened band suddenly weakens after 700 °C , in good agreement with the decomposition mechanism of $\text{Na}_3\text{V}_2(\text{PO}_4)_3$ at high temperature shown in Equation (3).

The characteristic Raman peaks are located at 1327 , 1587 , and 2654 cm^{-1} (Figure S5a, Supporting Information), corresponding to the D, G, and 2D bands of carbonaceous materials, respectively. It has been reported that the relative intensity ratio of D and G bands (ID/IG) indicates degree of crystallinity in various carbon materials.^[25] The ID/IG of each tablet samples is larger than 1, indicating the amorphous nature of carbon. The amount of carbon is estimated to be approximately 6% in the tablet samples (Figure S3b, Supporting Information) from the weight loss in air flow. The morphology of tablet samples is exhibited in Figure S3 in the Supporting Information. It is clear that all compounds composed of agglomerated nanoparticles, with secondary particle sizes mainly distributed around $1.5\text{ }\mu\text{m}$. The nanoparticles clinging to secondary particles surface of tablet samples calcined above 600 °C might be ascribed to chemical reaction between $\text{Na}_3\text{V}_2(\text{PO}_4)_2\text{F}_3$ and VPO_4 and decomposition process of $\text{Na}_3\text{V}_2(\text{PO}_4)_3$. In contrast to stable P element, the amount of F element declines steadily after 600 °C (Figure S4, Supporting Information), in good agreement with Equation (2). HRTEM images confirm the composite structure of crystalline particles and

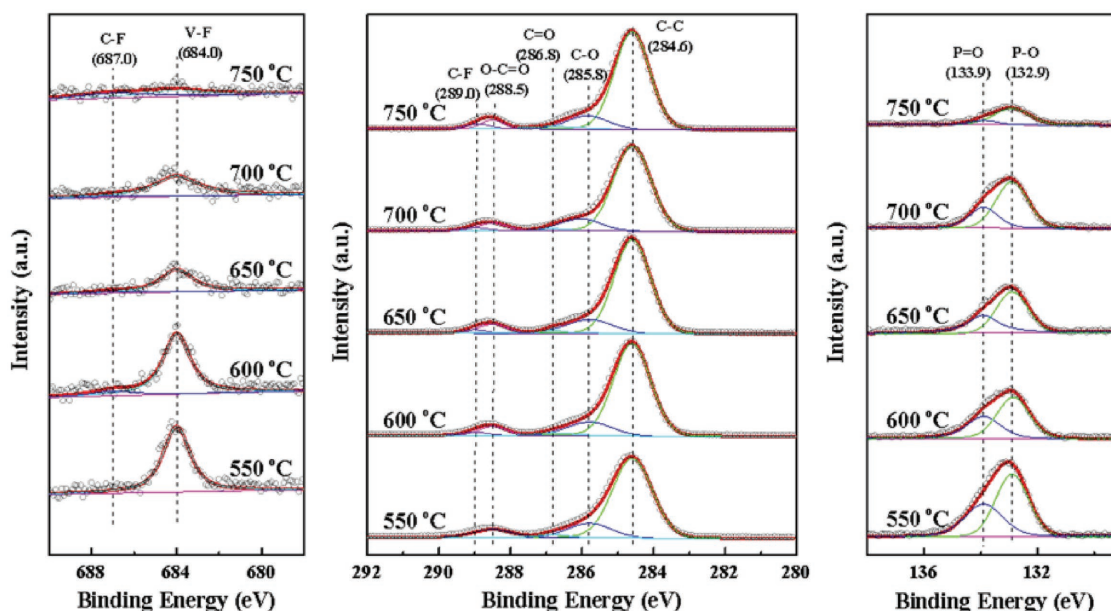


Figure 5. XPS spectra of F 1s, C 1s, and P 2p for tablet samples calcined at 550–750 °C.

amorphous carbon. As shown in **Figure 6**, all sample surfaces are well coated by amorphous carbon layer thinner than 5 nm, especially in TS550 and TS650, revealing that the fluorine escaped from $\text{Na}_3\text{V}_2(\text{PO}_4)_2\text{F}_3$ lattice could be scavenged by the carbon layers. The lattice fringe of 5.35 Å can be observed inside the particles in TS550, consistent with the interplanar spacing of (002) plane of $\text{Na}_3\text{V}_2(\text{PO}_4)_2\text{F}_3$, which demonstrates that TS550 is mainly composed of $\text{Na}_3\text{V}_2(\text{PO}_4)_2\text{F}_3$ particles. As for TS650, the crystallization region is obviously divided into two parts: a highly crystalline layered structure with a layer distance of 5.35 Å corresponding

to interplanar spacing of (002) plane of $\text{Na}_3\text{V}_2(\text{PO}_4)_2\text{F}_3$ on the left side, and another crystalline particle with fringe spacing of 3.73 Å consistent with (002) plane of $\text{Na}_3\text{V}_2(\text{PO}_4)_3$ on right side. Four divided parts of the multicomponent TS750 are shown in **Figure 6c**. On the basis of relevant fast Fourier transformation (FFT) images, crystal in part A can be ascribed to the newly formed $\text{Na}_3\text{V}_2(\text{PO}_4)_3$ particles; crystal in part B can be attributed to the residual $\text{Na}_3\text{V}_2(\text{PO}_4)_2\text{F}_3$ particles; amorphous layer in part C can be established as the coating carbon layer; and empty region in part D is gap of the transmission electron microscopy

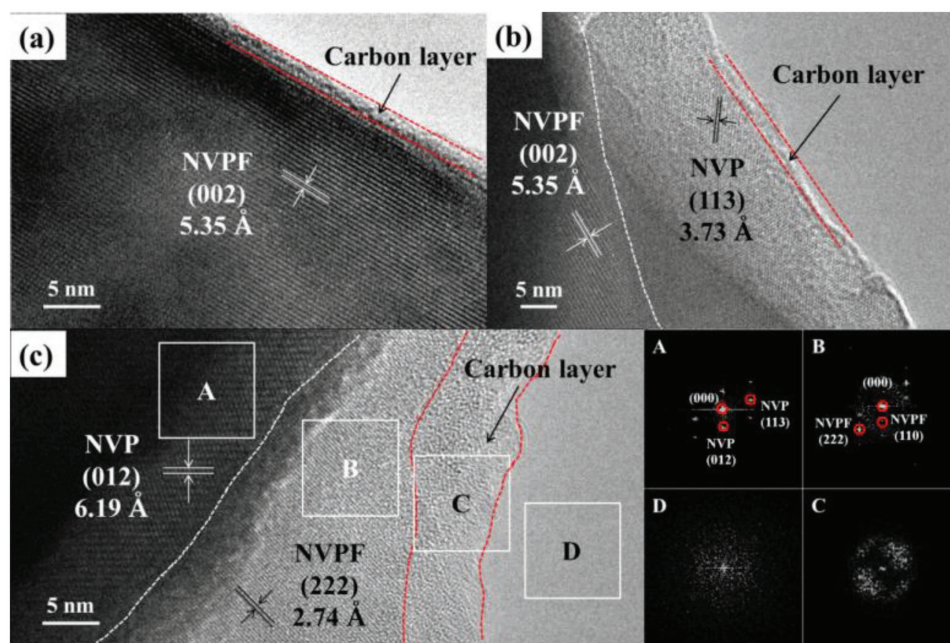


Figure 6. HRTEM images of tablet samples calcined at a) 550, b) 650, and c) 750 °C and FFT pictures correspond to the selected areas. The abbreviations of NVPF and NVP correspond to $\text{Na}_3\text{V}_2(\text{PO}_4)_2\text{F}_3$ and $\text{Na}_3\text{V}_2(\text{PO}_4)_3$.

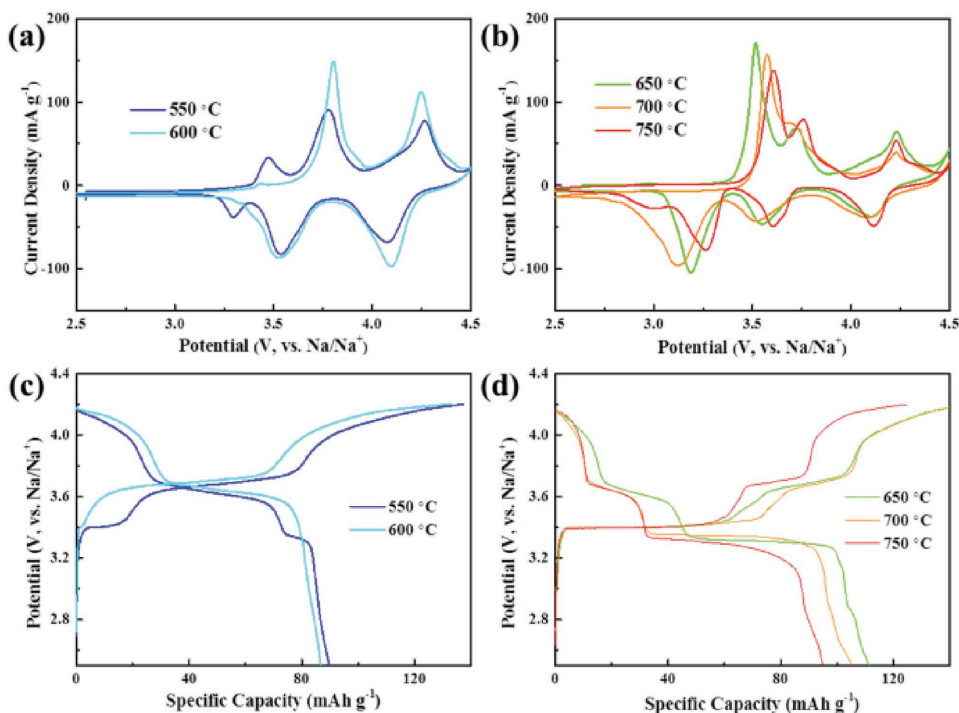


Figure 7. CV and the first cycle charge and discharge curves of tablet samples calcined at a,c) 550–600 °C and b,d) 650–750 °C.

(TEM) micro grid copper network. These results have recorded the process of constant loss of $\text{Na}_3\text{V}_2(\text{PO}_4)_2\text{F}_3$ and new generation of $\text{Na}_3\text{V}_2(\text{PO}_4)_3$ crystals, consistent with Equations (1) and (2).

CR2016 coin cells with Na metal anode were assembled to investigate the detailed electrochemical performance of tablet and powder samples. **Figure 7** shows the cyclic voltammetry (CV) curves of samples tested in potential range of 2.5–4.5 V (vs Na/Na^+) at a scan rate of $0.1 \text{ mV} \cdot \text{s}^{-1}$. When the temperature is elevated up to 550 and 600 °C, the samples exhibit two couples of redox peaks ($\approx 4.3 \text{ V}/4.1 \text{ V}$ and $3.8 \text{ V}/3.6 \text{ V}$ vs Na/Na^+) which belong to $\text{Na}_3\text{V}_2(\text{PO}_4)_2\text{F}_3$, and a couple of small redox peaks around $3.4 \text{ V}/3.3 \text{ V}$ (vs Na/Na^+) is attributed to $\text{Na}_3\text{V}_2(\text{PO}_4)_3$ for TS550. It demonstrates that the main active materials calcined below 650 °C is the well-established $\text{Na}_3\text{V}_2(\text{PO}_4)_2\text{F}_3$. However, a couple of strong redox peaks of $\approx 3.4 \text{ V}/3.3 \text{ V}$ (vs Na/Na^+) which belong to $\text{Na}_3\text{V}_2(\text{PO}_4)_3$ arise when temperature increased above 600 °C. Besides, another small and broad redox peaks around 2.9 V (vs Na/Na^+) are observed, belonging to the decomposition product of $\text{Na}_3\text{V}_2(\text{PO}_4)_3$.^[18] The redox peaks of $\text{Na}_3\text{V}_2(\text{PO}_4)_2\text{F}_3$ ($\approx 4.3 \text{ V}/4.1 \text{ V}$ and $3.8 \text{ V}/3.6 \text{ V}$ vs Na/Na^+) and $\text{Na}_3\text{V}_2(\text{PO}_4)_3$ ($\approx 3.4 \text{ V}/3.3 \text{ V}$ vs Na/Na^+) become weaker during elevated sintering temperature above 650 °C, whereas the small redox peaks around 2.9 V (vs Na/Na^+) become even larger.^[18] The corresponding charge/discharge curves at 0.1 C-rate (0.1 C means full charge/discharge in 10 h) are presented in Figure 7c,d. The initial charge/discharge curves of the test cells deliver an initial discharge capacity of 89.7, 86.7, 111.4, 105.3, and 94.9 mA h g^{-1} of TS550, TS600, TS650, TS700, and TS750. The specific charge and discharge potential plateaus (3.5 V/3.3 V vs Na/Na^+) capacity of $\text{Na}_3\text{V}_2(\text{PO}_4)_3$ increases at first and then decreases at temperatures above 650 °C. These results indicate that chemical reaction between $\text{Na}_3\text{V}_2(\text{PO}_4)_2\text{F}_3$ and VPO_4 and

decomposition reaction of $\text{Na}_3\text{V}_2(\text{PO}_4)_3$ occur at same time when the temperature increases up to 650 °C. The charge and discharge curves of powder samples (Figure S6, Supporting Information) show there is a diminishing trend in plateaus of $\text{Na}_3\text{V}_2(\text{PO}_4)_2\text{F}_3$. The difference of charge and discharge curves between tablet and powder samples illustrates that compacted tablet blocks the continuous reaction between $\text{Na}_3\text{V}_2(\text{PO}_4)_2\text{F}_3$ and VPO_4 and hinders the fleeing of fluorine.

Based on our experience, with 1:1 NaF: VPO_4 feedstock and solid-state synthesis one cannot get single-phase NaVPO_4F compound at any temperature. Instead, one gets two-phase mixture of $\text{Na}_3\text{V}_2(\text{PO}_4)_2\text{F}_3 + \text{VPO}_4$ up to 500 °C. The resulting tetragonal $P4_2/mnm$ /subtle orthorhombic ($b/a = 1.002$) $Amam$ $\text{Na}_3\text{V}_2(\text{PO}_4)_2\text{F}_3$ may be easily mistaken to be tetragonal $I4/mmm$.^[3a] And then from 600 to 800 °C, $\text{Na}_3\text{V}_2(\text{PO}_4)_2\text{F}_3 + \text{VPO}_4 \rightarrow \text{Na}_3\text{V}_2(\text{PO}_4)_3 + \text{VF}_3 \uparrow$. The degree of VF_3 volatilization depends on the temperature exposure and details of pelletization; however, some vaporization of VF_3 and mass loss are unavoidable after 650 °C. Since $\text{Na}_3\text{V}_2(\text{PO}_4)_3$ is rhombohedral $R\bar{3}c$, it may also be easily mistaken to be nontavorite monoclinic C_2/c NaVPO_4F .^[6,11] Based on Barker and co-workers and Zhao and co-workers,^[3a,6] many researchers have quoted tetragonal $I4/mmm$ and nontavorite monoclinic C_2/c NaVPO_4F from solid-state synthesis; for example, Zhao and co-workers reported a gradual phase transition of NaVPO_4F from monoclinic at 700 °C to tetragonal at 750 °C;^[7] however, we believe these assignments of single-phase NaVPO_4F compound may often be mistaken.

Since we have not obtained NaVPO_4F with solid-state synthesis, we would like to form NaVPO_4F by another method, liquid-aided electrochemical ion exchange. We perform $\text{Li} \rightarrow \text{Na}$ ion exchange on LiVPO_4F , by introducing LiVPO_4F as cathode to cycle in a sodium half-cell to form NaVPO_4F electrochemically for

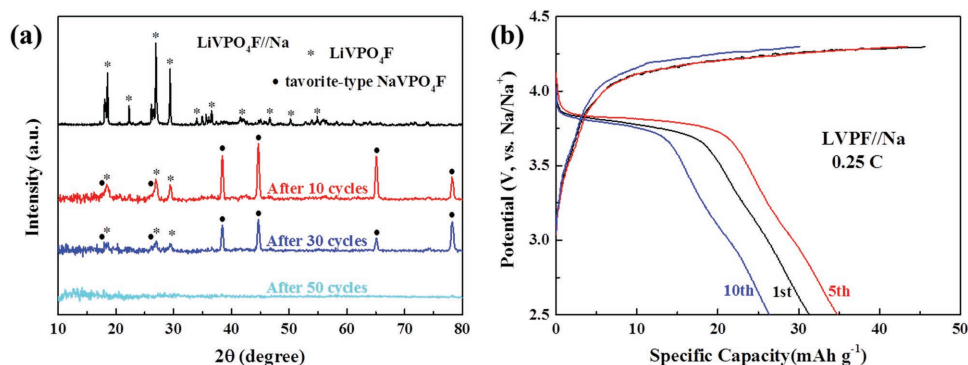


Figure 8. a) XRD patterns of LiVPO_4F and the ion exchange compound after 10, 30, and 50 cycles in a sodium cell; b) The 1st, 5th, and 10th charge and discharge curves of LiVPO_4F in sodium cell with a potential window of 2.5–4.3 V (vs Na/Na^+).

comparison.^[17,26] As shown in **Figure 8**, the XRD patterns of LiVPO_4F and the ion exchanged compound after 10, 30, and 50 cycles are well observed. After 10 cycles' electrochemical ion exchange process, Na ions are expected to be the cations reinserted into VPO_4F framework due to preponderant Na ion concentration in sodium half-cell. The crystal structure has changed dramatically after 10 cycles which can be ascribed to the formation of NaVPO_4F . However, this new structure of NaVPO_4F by liquid-phase method is far different from the hypothetical tetragonal I_4/mmm and nontavorite C_2/c NaVPO_4F of previous reports (in the sense that although no explicit atomic coordinates were given and of a different stoichiometry, they were all acclaimed to be as similar to Le Meins' family).^[3a,4,6] These liquid-phase NaVPO_4F belongs to the Tavorite family instead.^[3a,6–8,9b,12,16,27] Furthermore, a unique and distinct charge/discharge plateaus at ≈ 3.9 V (vs Na/Na^+) is detected in charge and discharge curves (**Figure 8b**), which is different from the tetragonal (4.1 and 3.6 V vs Na/Na^+) and nontavorite monoclinic “ NaVPO_4F ” (3.4 V vs Na/Na^+),^[3a,6–8,9b,16,27] now strongly suspected to be multiphase mixtures of Le Meins' $\text{Na}_3\text{V}_2(\text{PO}_4)_2\text{F}_3$, VPO_4 , and $\text{Na}_3\text{V}_2(\text{PO}_4)_3$. Therefore, we would like to suggest that the tetragonal NaVPO_4F and nontavorite monoclinic NaVPO_4F are probably wrong assignments in previous cognitions,^[3a,6] while tavorite-type NaVPO_4F (by electrochemical ion exchange) and tetragonal $P4_2/mnm$ /subtly orthorhombic ($b/a = 1.002$) $Amam$ $\text{Na}_3\text{V}_2(\text{PO}_4)_2\text{F}_3$ (by solid-state synthesis) can truly be formed. This multi-phase mixture theory also explains why Barker's “ NaVPO_4F ” gave only 82 mAh g^{-1} in 2003,^[3a] while the single-phase $\text{Na}_3\text{V}_2(\text{PO}_4)_2\text{F}_3$ gave $115\text{--}120 \text{ mAh g}^{-1}$ reversible capacity^[3b] in 2006.

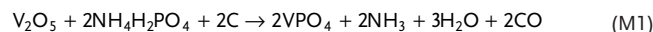
3. Conclusions

Careful analysis of in situ XRD during the solid-state synthesis of raw materials (NaF and VPO_4 mixture with proportion of 1:1) provides insight into the reaction and formation mechanism of tetragonal $P4_2/mnm$ /subtly orthorhombic ($b/a = 1.002$) $Amam$ $\text{Na}_3\text{V}_2(\text{PO}_4)_2\text{F}_3$ of Le Meins' family, but not NaVPO_4F . 3:2 reaction of $\text{NaF}:\text{VPO}_4$ into $\text{Na}_3\text{V}_2(\text{PO}_4)_2\text{F}_3$ occurred first at 400°C ; 1:1 chemical reaction between $\text{Na}_3\text{V}_2(\text{PO}_4)_2\text{F}_3:\text{VPO}_4$ was observed at 700°C , but instead of forming NaVPO_4F as one might expect, due to volatilization of VF_3 , $\text{Na}_3\text{V}_2(\text{PO}_4)_3$ was formed; decomposition of $\text{Na}_3\text{V}_2(\text{PO}_4)_3$ was discovered at 850°C . The

tablet and powder samples calcined at various temperatures convincingly demonstrate these three reactions, in addition to the different reaction temperatures with longtime insulation. Liquid-phase electrochemical ion exchange of LiVPO_4F provides the tavorite-type NaVPO_4F , far from the hypothetical tetragonal and nontavorite monoclinic NaVPO_4F structures reported previously, or Le Meins' family $\text{Na}_3\text{V}_2(\text{PO}_4)_2\text{F}_3$. The results presented here clarify the misunderstandings and illustrate that tetragonal NaVPO_4F (space group I_4/mmm) probably does not exist. Moreover, due to the major weight loss, nontavorite monoclinic NaVPO_4F might be misleading. These structures might be multiphase mixtures of Le Meins' $\text{Na}_3\text{V}_2(\text{PO}_4)_2\text{F}_3$, unreacted VPO_4 and hexagonal $\text{Na}_3\text{V}_2(\text{PO}_4)_3$ instead. The understanding gained about the formation mechanism upon heating process of 1:1 $\text{NaF}:\text{VPO}_4$ raw materials we proposed may help us avoid future mislabeling of fluorophosphate SIB cathode materials.

4. Experimental Section

Materials Preparation: The active materials calcined at different temperatures were prepared by a traditional two-step carbothermal reduction route. V_2O_5 and $\text{NH}_4\text{H}_2\text{PO}_4$ with a stoichiometric amount were first ball milled with acetylene black (20% excess) in 400 rpm for 6 h to get a uniform particles distribution. The mixture was calcined at 750°C for 8 h in argon (Ar) atmosphere to obtain VPO_4 . The active materials were prepared by mixing and tablet or not with proportion (1:1) of the intermediate VPO_4 and NaF , then sintered at 550, 600, 650, 700, and 750°C under Ar flow for 8 h, respectively. The first step incorporation reaction may be summarized as



The unexhausted acetylene black was left as carbon coating on the surface of the active materials in the final product.

Characterization: In situ and ex situ XRD measurement was performed to characterize the structural and compositional evolution upon heating by using an X'pert Pro (PANalytical Ltd., Holland) with $\text{Cu K}\alpha$ radiation ($\lambda = 1.5406 \text{ \AA}$). Characteristic weight loss and thermodynamic heat energy transmission of the second step mixture precursor were measured by TGA/DSC analyses using a Mettler Toledo (TGA/DSC 1) thermoanalyzer. The measurement was conducted from room temperature to 900°C at a heating rate of $10^\circ\text{C min}^{-1}$. The IR spectra were obtained by FTIR spectrometer (Nicolet, iS10, USA) under transmission mode based on the KBr pellet method in the range of $400\text{--}4000 \text{ cm}^{-1}$. XPS was collected by using a monochromatic $\text{Al K}\alpha$ (1486.6 eV) radiation. Raman spectra were obtained on a HORIBA JOBIN YVON micro-Raman spectrometer.

The particle morphology of the active materials (heat treatment at 550–750 °C, at an interval of 50 °C, in the second step) was observed by field emission scanning electron microscopy (FE-SEM Quanta 250FEG, FEI, USA). TEM (TEM, FEI TITAN G2, USA) was employed to characterize the morphology as well as the evolution of raw materials upon heating.

Electrochemical Measurement: The electrochemical performance was carried out with 2016 coin cells assembled in glove box filled with high-purity argon gas. In the sodium half-cells, the 70% active material, 20% conducting carbon (super P), and 10% polyvinylidene fluoride binder (PVDF) were used as the cathode, a microporous polymer (Celgard 2500) as separator, the sodium metal as the anode, and 1 M solution of NaClO₄ in EC-DMC (50:50) as the electrolyte. The mass loading of active material in each coin cell is typically 1.0–1.5 mg cm⁻², and the electrode footprint area is 2.01 cm². The galvanostatic charge/discharge at the range of 2.5–4.2 V vs Na/Na⁺ was measured on a CT2001A Land Battery Testing System, while the CV was performed on a Versatile Multichannel Galvanostat 2/Z (VMP2, Princeton Applied Research).

Supporting Information

Supporting Information is available from the Wiley Online Library or from the author.

Acknowledgements

This work was financially supported by the National Natural Science Foundation of China (Grant No. 21503158), the National Natural Science Foundation of China (Grant No. 51772240), the Key Research and Development Plan of Shaanxi Province (China, 2017ZDCXL-GY-08-02), the Natural Science Foundation of Shaanxi Province (China, Grant No. 2014JQ2-2007), the 111 Project (B14040), and the Fundamental Research Funds for the Central Universities of China (Grant No. xjj2014044). The SEM/TEM work was done at the International Center for Dielectric Research (ICDR), Xi'an Jiaotong University, Xi'an, China; the authors also thank Lu Lu for her help in using TEM. J.L. acknowledges support by NSF ECCS-1610806.

Conflict of Interest

The authors declare no conflict of interest.

Keywords

Na₃V₂(PO₄)₃, tavorite-type NaVPO₄F, volatile VF₃ gas

Received: April 7, 2018

Revised: May 16, 2018

Published online:

- [1] a) E. C. Everts, *Nature* **2015**, 526, S93; b) H. Hongshuai, S. Lidong, Z. Yan, Z. Guoqiang, C. Jun, J. Xiaobo, *Adv. Sci.* **2017**, 4, 1600243; c) H. Hou, C. E. Banks, M. Jing, Y. Zhang, X. Ji, *Adv. Mater.* **2015**, 27, 7861.
- [2] Q. Ni, Y. Bai, F. Wu, C. Wu, *Adv. Sci.* **2017**, 4, 1600275.
- [3] a) J. Barker, M. Y. Saïdi, J. L. Swoyer, *Electrochim. Solid-State Lett.* **2003**, 6, A1; b) J. Barker, R. K. B. Gover, P. Burns, A. J. Bryan, *Electrochim. Solid-State Lett.* **2006**, 9, A190.
- [4] J. M. Le Meins, M. P. Crosnier-Lopez, A. Hemon-Ribaud, G. Courbion, *J. Solid State Chem.* **1999**, 148, 260.

- [5] C. Delacourt, L. Laffont, R. Bouchet, C. Wurm, J. B. Leriche, M. Morcrette, J. M. Tarascon, C. Masquelier, *J. Electrochem. Soc.* **2005**, 152, A913.
- [6] H. Zhuo, X. Wang, A. Tang, Z. Liu, S. Gamboa, P. J. Sebastian, *J. Power Sources* **2006**, 160, 698.
- [7] J. Zhao, J. He, X. Ding, J. Zhou, Y. o. Ma, S. Wu, R. Huang, *J. Power Sources* **2010**, 195, 6854.
- [8] M. Xu, C.-J. Cheng, Q.-Q. Sun, S.-J. Bao, Y.-B. Niu, H. He, Y. Li, J. Song, *RSC Adv.* **2015**, 5, 40065.
- [9] a) Y.-L. Ruan, K. Wang, S.-D. Song, X. Han, B.-W. Cheng, *Electrochim. Acta* **2015**, 160, 330; b) T. Jin, Y. C. Liu, Y. Li, K. Z. Cao, X. J. Wang, L. F. Jiao, *Adv. Energy Mater.* **2017**, 7, 1700087.
- [10] M. Law, P. Balaya, *Energy Storage Mater.* **2018**, 10, 102.
- [11] Z.-m. Liu, X.-y. Wang, Y. Wang, A.-p. Tang, S.-y. Yang, L.-f. He, *Trans. Nonferrous Met. Soc. China* **2008**, 18, 346.
- [12] E. Boivin, J. N. Chotard, T. Bamine, D. Carlier, P. Serras, V. Palomares, T. Rojo, A. Iadecola, L. Dupont, L. Bourgeois, F. Fauth, C. Masquelier, L. Croguennec, *J. Mater. Chem. A* **2017**, 5, 25044.
- [13] a) M. Bianchini, F. Fauth, N. Brisset, F. Weill, E. Suard, C. Masquelier, L. Croguennec, *Chem. Mater.* **2015**, 27, 3009; b) I. Spanopoulos, W. Ke, C. C. Stoumpos, E. C. Schueller, O. Y. Kontsevoi, R. Seshadri, M. G. Kanatzidis, *J. Am. Chem. Soc.* **2018**, 140, 5728; c) A. L. Balch, K. Winkler, *Chem. Rev.* **2016**, 116, 3812.
- [14] F. Sauvage, E. Quarez, J. M. Tarascon, E. Baudrin, *Solid State Sci.* **2006**, 8, 1215.
- [15] a) S. Li, Y. Dong, L. Xu, X. Xu, L. He, L. Mai, *Adv. Mater.* **2014**, 26, 3545; b) J.-N. Chotard, G. Rousse, R. David, O. Mentré, M. Courty, C. Masquelier, *Chem. Mater.* **2015**, 27, 5982; c) Y. Fang, L. Xiao, X. Ai, Y. Cao, H. Yang, *Adv. Mater.* **2015**, 27, 5895; d) K. Saravanan, C. W. Mason, A. Rudola, K. H. Wong, P. Balaya, *Adv. Energy Mater.* **2013**, 3, 444.
- [16] Y. Lu, S. Zhang, Y. Li, L. Xue, G. Xu, X. Zhang, *J. Power Sources* **2014**, 247, 770.
- [17] J.-M. Ateba Mba, C. Masquelier, E. Suard, L. Croguennec, *Chem. Mater.* **2012**, 24, 1223.
- [18] W. Song, X. Ji, Y. Yao, H. Zhu, Q. Chen, Q. Sun, C. E. Banks, *PCCP* **2014**, 16, 3055.
- [19] a) J. Meng, H. Guo, C. Niu, Y. Zhao, L. Xu, Q. Li, L. Mai, *Joule* **2017**, 1, 522; b) A. Wang, S. Kadam, H. Li, S. Shi, Y. Qi, *npj Comput. Mater.* **2018**, 4, 15.
- [20] a) A. Paoletta, G. Bertoni, E. Dilena, S. Marras, A. Ansaldo, L. Manna, C. George, *Nano Lett.* **2014**, 14, 1477; b) M. J. Aragón, P. Lavela, G. F. Ortiz, J. L. Tirado, *ChemElectroChem* **2015**, 2, 995.
- [21] Y. Qi, L. Mu, J. Zhao, Y.-S. Hu, H. Liu, S. Dai, *Angew. Chem., Int. Ed.* **2015**, 54, 9911.
- [22] a) M. E. Holtz, Y. Yu, D. Gunceler, J. Gao, R. Sundararaman, K. A. Schwarz, T. A. Arias, H. D. Abruña, D. A. Muller, *Nano Lett.* **2014**, 14, 1453; b) A. Ait Salah, P. Jozwiak, K. Zaghib, J. Garbarczyk, F. Gendron, A. Mauger, C. M. Julien, *Spectrochim. Acta, Part A* **2006**, 65, 1007; c) N. Suzuki, W. D. Richards, Y. Wang, L. J. Miara, J. C. Kim, I.-S. Jung, T. Tsujimura, G. Ceder, *Chem. Mater.* **2018**, 30, 2236; d) B. L. Corso, I. Perez, T. Sheps, P. C. Sims, O. T. Gül, P. G. Collins, *Nano Lett.* **2014**, 14, 1329.
- [23] a) R. Zhang, X. Chen, X. Shen, X.-Q. Zhang, X.-R. Chen, X.-B. Cheng, C. Yan, C.-Z. Zhao, Q. Zhang, *Joule* **2018**, 2, 764; b) J. Zhang, W. Lv, D. Zheng, Q. Liang, D.-W. Wang, F. Kang, Q.-H. Yang, *Adv. Energy Mater.* **2018**, 8, 1702395.
- [24] J. Ren, Y. Zhang, W. Bai, X. Chen, Z. Zhang, X. Fang, W. Weng, Y. Wang, H. Peng, *Angew. Chem., Int. Ed. Engl.* **2014**, 53, 7864.
- [25] Y. H. Jung, C. H. Lim, D. K. Kim, *J. Mater. Chem. A* **2013**, 1, 11350.
- [26] a) X. Sun, Y. Xu, M. Jia, P. Ding, Y. Liu, K. Chen, *J. Mater. Chem. A* **2013**, 1, 2501; b) C. Yang, X. Ji, X. Fan, T. Gao, L. Suo, F. Wang, W. Sun, J. Chen, L. Chen, F. Han, L. Miao, K. Xu, K. Gerasopoulos, C. Wang, *Adv. Mater.* **2017**, 29.
- [27] C. Chang, Y. Li, W. He, G. Li, W. Guo, P. Zhu, M. Yao, J. Feng, *Mater. Lett.* **2017**, 209, 82.

ADVANCED ENERGY MATERIALS

Supporting Information

for *Adv. Energy Mater.*, DOI: 10.1002/aenm.201801064

Fluorophosphates from Solid-State Synthesis and
Electrochemical Ion Exchange: NaVPO_4F or $\text{Na}_3\text{V}_2(\text{PO}_4)_2\text{F}_3$?

Long Li, Youlong Xu, Xiaofei Sun, Rui Chang, Yuan Zhang,
Xiaona Zhang, and Ju Li**

Supplementary information

Fluorophosphates from Solid-State Synthesis and Electrochemical Ion Exchange: NaVPO_4F or $\text{Na}_3\text{V}_2(\text{PO}_4)_2\text{F}_3$?

Long Li^{1,2}, Youlong Xu^{1,2,*}, Xiaofei Sun^{1,2}, Rui Chang², Yuan Zhang^{1,2}, Xiaona Zhang^{1,2}, Ju Li^{3,*}

¹Electronic Materials Research Laboratory, Key Laboratory of the Ministry of Education & International Center for Dielectric Research, Xi'an Jiaotong University, Xi'an 710049 PR China

²Shaanxi Engineering Research Center of Advanced Energy Materials & Devices, Xi'an Jiaotong University, Xi'an, China

³Department of Nuclear Science and Engineering and Department of Materials Science and Engineering, Massachusetts Institute of Technology Cambridge, MA 02139

*Corresponding author: ylxu@mail.xjtu.edu.cn (Youlong Xu)

liju@mit.edu (Ju Li)

Figures

Figure S1 (a) Rietveld refinement based on the XRD pattern of the precursor phase. (b) XRD patterns of the powder samples calcined at 550 - 750 °C. (c) and (d) XRD patterns of raw materials with various ratio of NaF and VPO_4 calcined at 600 °C in 3D and 2D mode, respectively.

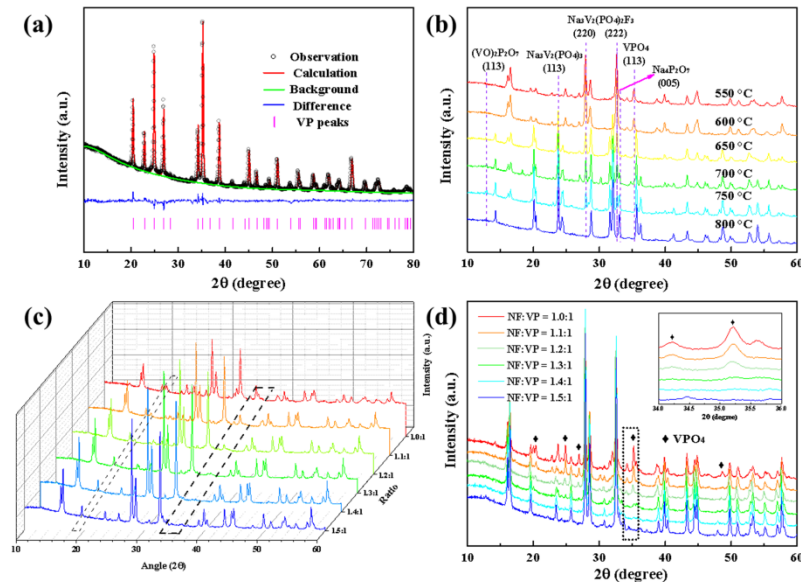


Figure S2 FT-IR spectra of powder samples calcined at 550 - 750 °C.

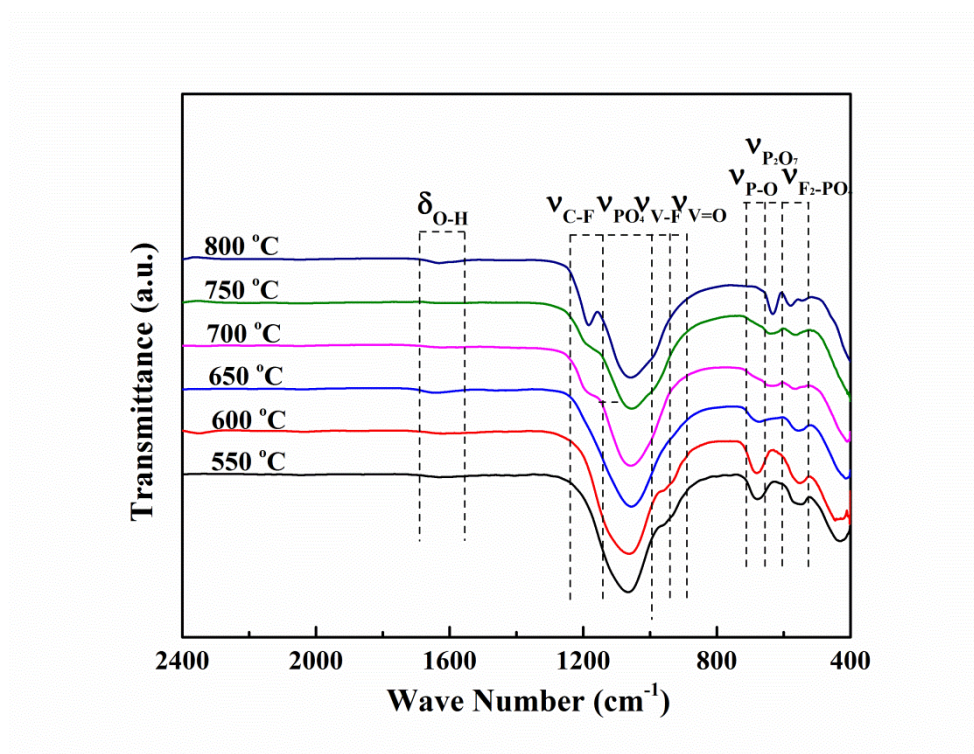


Figure S3 (a) Raman spectra of tablet samples calcined at 550 - 750 °C. (b) TG curves of tablet samples from 50 °C to 600 °C at a heating rate of 10 °C min⁻¹ in Air flow.

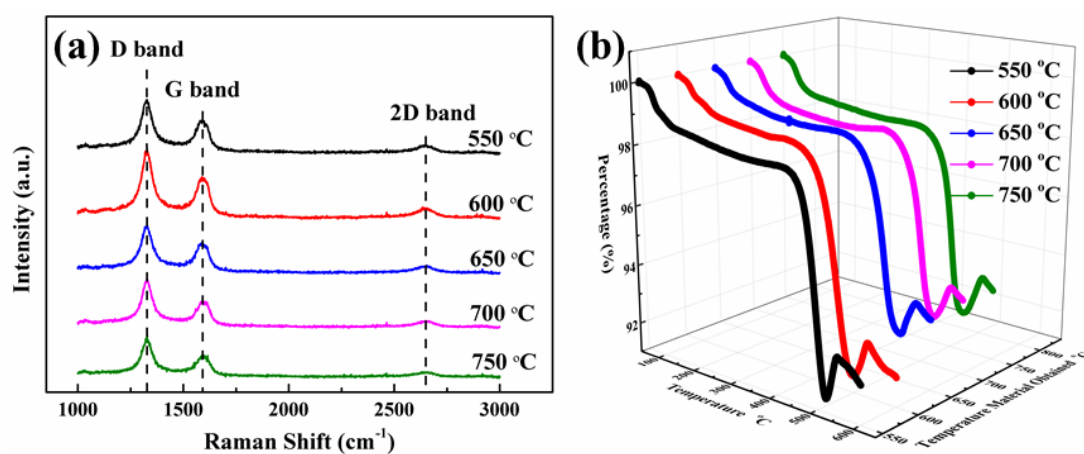


Figure S4 FESEM images of tablet samples calcined at 550 - 750 °C.

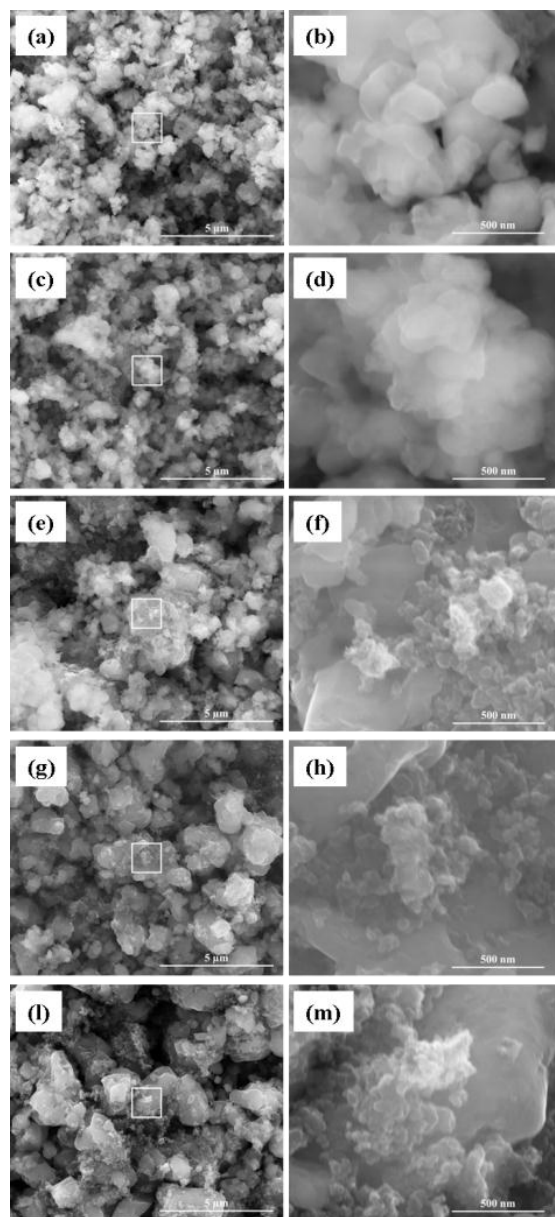


Figure S5 EDS element analysis (a) – (e) and the percentage of F and P element (f) of tablet samples calcined at 550 - 750 °C.

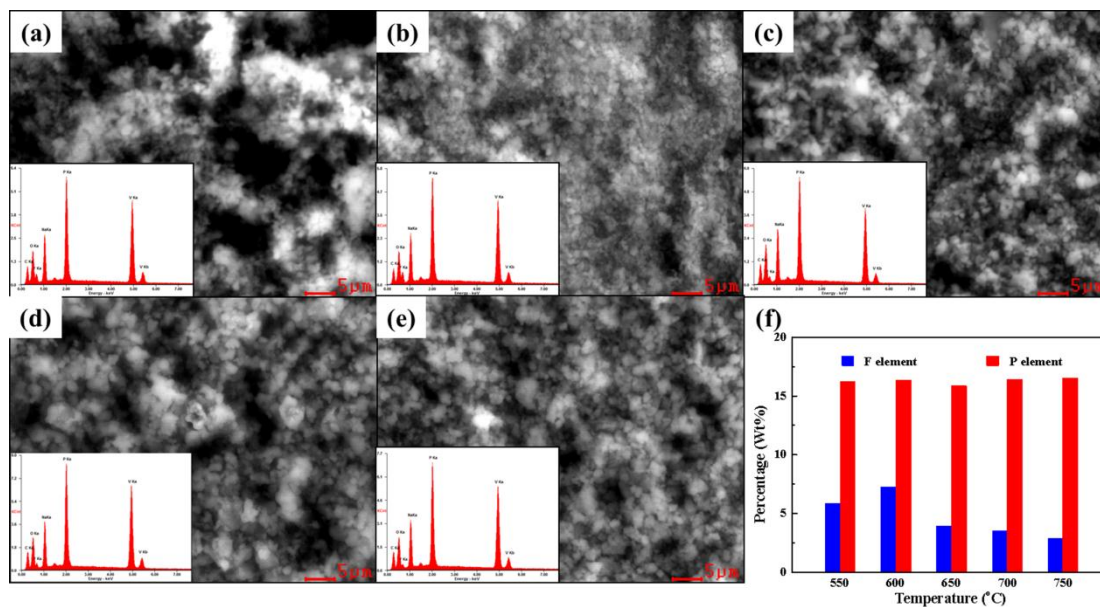
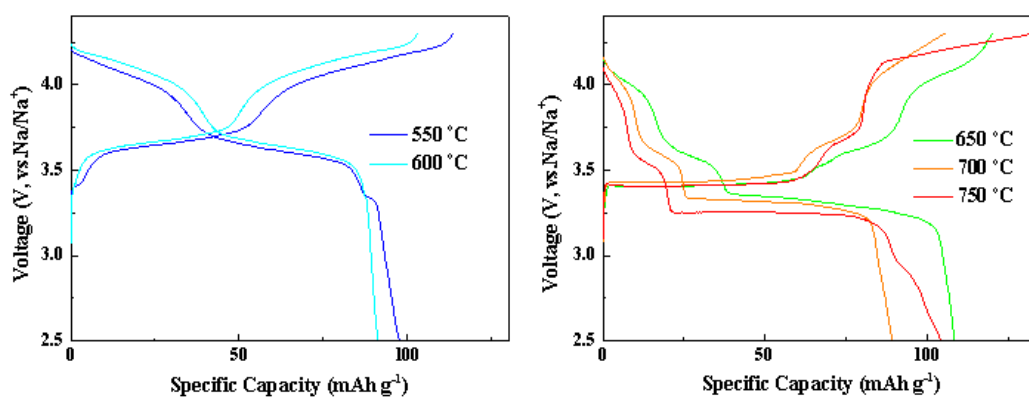


Figure S6 The charge/discharge curves of powder samples calcined at 550 - 750 °C. The load density of the electrode is about 1.5 ~2.0 mg cm⁻², with the formulation of active materials: acetylene black: PVDF = 70: 20:10 (weight).



Tables

Table S1 The compositional changes of raw material upon heating calculated by semi-quantitative calculation of in situ XRD patterns.

Temperature	NaF (at%)	VPO ₄ (at%)	Na ₃ V ₂ (PO ₄) ₂ F ₃ (at%)	Na ₃ V ₂ (PO ₄) ₃ (at%)	Na ₄ P ₂ O ₇ (at%)	(VO) ₂ P ₂ O ₇ (at%)
25	46	54	0	0	0	0
300	41	59	0	0	0	0
400	19	57	24	0	0	0
450	0	53	47	0	0	0
500	0	51	49	0	0	0
550	0	52	48	0	0	0
600	0	48	52	0	0	0
650	0	50	50	0	0	0
700	0	20	20	60	0	0
750	0	14	14	72	0	0
800	0	0	0	100	0	0
850	0	0	0	91	7	2
900	0	0	0	88	9	3
950	0	0	0	85	11	4